J. Astrophys. Astr. (1999) **20**, 1–22

Understanding the Spectral Energy Distributions of the Galactic Star Forming Regions IRAS 18314–0720, 18355–0532 and 18316–0602

Bhaswati Mookerjea & S. K. Ghosh, *Tata Institute of Fundamental Research, Homi Bhabha Road, Colaba, Mumbai (Bombay) 400 005, India*

Received 1998 August 5; accepted 1999 June 17

Abstract. Embedded Young Stellar Objects (YSO) in dense interstellar clouds are treated self-consistently to understand their spectral energy distributions (SED). Radiative transfer calculations in spherical geometry involving the dust as well as the gas component, have been carried out to explain observations covering a wide spectral range encompassing near-infrared to radio continuum wavelengths. Various geometric and physical details of the YSOs are determined from this modelling scheme.

In order to assess the effectiveness of this self-consistent scheme, three young Galactic star forming regions associated with IRAS 18314–0720, 18355–0532 and 18316–0602 have been modelled as test cases. They cover a large range of luminosity (≈ 40). The modelling of their SEDs has led to information about various details of these sources, e.g. embedded energy source, cloud structure and size, density distribution, composition and abundance of dust grains etc. In all three cases, the best fit model corresponds to the uniform density distribution. Two types of dust have been considered, viz., Draine & Lee (DL) and the Mezger, Mathis & Panagia (MMP). Models with MMP type dust explain the dust continuum and radio continuum emission from IRAS 18314–0720 and 18355–0532 self-consistently. These models predict much lower intensities for the fine structure lines of ionized heavy elements, than those observed for IRAS 18314–0720 and 18355–0532. This discrepancy has been resolved by invoking clumpiness in the interstellar medium. For IRAS 18316–0602, the model with DL type dust grains is preferred.

Key words. Infrared SED – HII regions – radiative transfer – IRAS 18314–0720 – IRAS 18355–0532 – IRAS 18316–0602.

1. Introduction

The formation and the initial stages of evolution of stars take place inside dense regions within molecular clouds, from which they are born. Hence, the star formation studies have necessarily to deal with the protostars/young stars in the environment of interstellar gas and dust from the parent cloud. The stars with sufficient supply of Lyman continuum photons (basically depending on their mass) create and maintain HII regions around them. The (ultra)/compact variety of HII regions in particular provides a natural test case for better understanding of medium/high mass star formation. They present two main advantages for such studies: being younger they

allow one to probe the physical processes closer in time to the formation of the embedded star, and secondly they have simpler geometrical shapes (e.g. with spherical/ cylindrical symmetry), thus providing opportunity for direct comparison between the observations and the predictions of detailed numerical models. In addition, being of the higher luminosity class (roughly between ZAMS O4 and B0.5), observationally they can be studied over larger distances (almost any part of the Galaxy) in the radio continuum as well as infrared/sub-mm. Available observational data regarding continuum emission from Galactic compact HII regions span a wide spectral range covering near-infrared (NIR) to sub-millimeter wavelengths. Whereas the atmospheric windows in NIR, sub-millimeter and a few restricted ones in the mid-IR (MIR) have been used extensively, the peak of the spectral energy distribution (SED) lies invariably in the far-IR (FIR) waveband which is inaccessible from the earth-based observatories. The work horse for the high angular resolution FIR measurements of Galactic star forming regions has been the Kuiper Airborne Observatory, occasionally supplemented by balloon-borne telescopes. Although the InfraRed Astronomy Satellite (IRAS) offers the only near all sky and most complete data base, its poorer angular resolution limits its usefulness, particularly for the study of compact HII regions. However, this situation is about to change drastically with the advent of the European Space Agency's Infrared Space Observatory (ISO) mission. ISO with improved photometric sensitivity as well as spectral and angular resolution, will open up enormous opportunity to perform detailed studies of Galactic star forming regions in the entire infrared waveband encompassing Near through Mid to Far Infrared. Most of the infrared continuum emission from the embedded YSOs originating from the interstellar dust component will be measured throughout the 2.5–200 μm region with greater photometric precision and with diffraction limited angular resolution, by the ISO instruments. In addition, the spectroscopic data will help understand the composition as well as physical parameters of the interstellar gas component.

Keeping the above in mind, the present study is a step in trying to establish a self-consistent yet simple scheme of modelling Galactic compact HII regions in spherically symmetric geometry. Here, by self-consistent we mean that the same geometric and physical configuration fits the observed data for the emission from the dust (most of the infrared, sub-mm, mm part of the SED) as well as the emission from the gas (radio continuum, fine structure line etc). The main aim is to extract maximum possible information regarding the geometric and physical details of the star forming region from the observed SED. In addition to predicting the continuum infrared emission from the dust, the gas component has also been integrated in a self consistent manner, thereby predicting the absolute and relative strengths of atomic/nebular lines as well as the radio continuum emission.

In order to assess the usefulness of the above scheme, three Galactic embedded YSOs (IRAS 18314–0720, 18355–0532 and 18316–0602; most likely in compact HII region phase, have been selected for modelling. These sources have been chosen based on availability of relevant observational data; and also to cover a wide range of total luminosity (a factor of ≈ 40). These three sources IRAS 18314–0720, 18355–0532 and 18316–0602 have luminosities 1.02×10^6, 1.4×10^5 and $2.5 \times 10^4 L_\odot$ respectively (which correspond to single ZAMS stars of type O4, O6.5 and B0). Although at this point of time the available amount of validated ISO data in public domain is rather limited, much more sophisticated application of this scheme is anticipated in the future.

The outline of this paper is as follows. Section 2 describes the modelling scheme including the treatments of radiative transfer in the dust and the gas components respectively. Section 3 presents the observational constraints of the three sources, and the results of modelling in the form of geometrical and physical information extracted about these sources. Conclusions are summarized in section 4.

2. The modelling scheme

A compact HII region is modelled as a spherically symmetric cloud (made of typical interstellar gas-dust material), powered by centrally embedded single or a cluster of zero age main sequence (ZAMS) star/(s). This cloud is assumed to be immersed in an isotropic radiation field (typical Interstellar Radiation Field, ISRF). The interstellar gas and the dust is assumed to follow the same radial density distribution law, but with the following difference—whereas the gas exists throughout the cloud (i.e. right from the stellar surface up to the outer boundary of the cloud, R_{max}; see Fig. 1), there is a natural lower limit to the inner boundary, R_{min}, for the dust distribution (i.e. a cavity in the dust cloud). This is because the dust grains are destroyed when exposed to excessive radiative heating. The gas to dust ratio, where they co-exist ($R_{min} < r < R_{max}$), is assumed to be constant. The position of the ionization front (R_{HII}, refer to Fig. 1) depends on the effective temperature and luminosity of

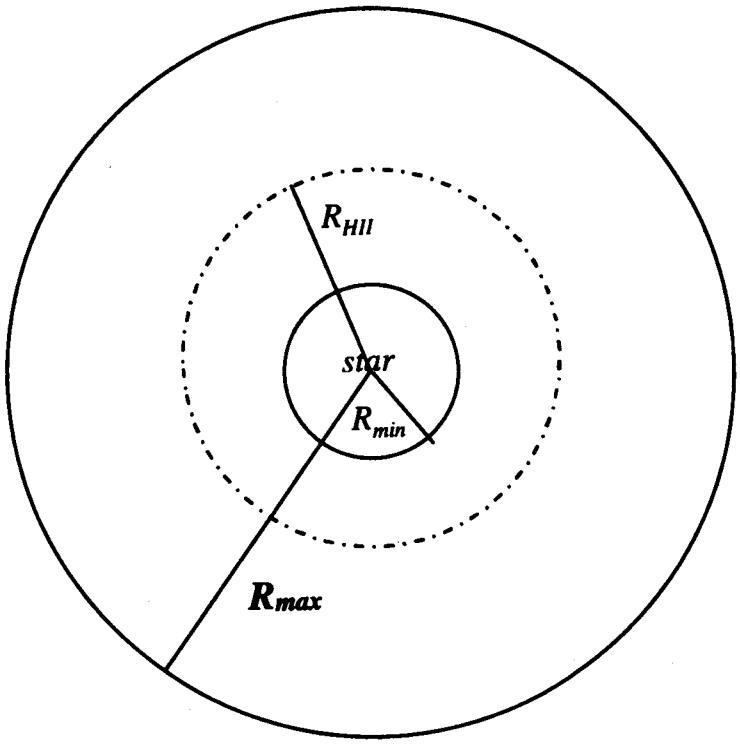

Figure 1. Schematic diagram of the model star forming region.

the exciting star, as well as the density of the gas. The case, $R_{\rm HII} < R_{\rm min}$ is also possible, if either the star is not hot enough and/or the density of gas around the star is quite high.

Modelling a specific compact HII region involves matching the predicted emergent spectral (continuum) shape with the measured SED and comparing the relative and absolute strengths of the atomic/nebular spectral lines from the gas component with spectroscopic observations (if available).

The following are the inputs for individual runs of the modelling scheme:

(i) the total luminosity;
(ii) the spectral shape of the radiation emerging from the embedded source/(s) (sensitive to the assumed Initial Mass Function and upper mass cut off, in case of a star cluster);
(iii) the gas to dust ratio;
(iv) the properties of the dust grains (of each type considered);
(v) the ISRF incident at the outer boundary;
(vi) the elemental abundances in the gas component (which is assumed to be uniform throughout the cloud).

The total luminosity of the embedded energy source/(s) is frozen at the value determined by integrating the observed continuum SED. The embedded energy source/(s) is varied between a single ZAMS star and a cluster of ZAMS stars. The canonical value of 100:1 for the gas to dust ratio by mass is used initially, but varied if no acceptable model can be constructed to fit all the data. Two types of dust have been considered here, that of Draine & Lee (1984; hereafter DL) and Mezger, Mathis & Panagia (1982; hereafter MMP). Within each type, dust consists of grains of different composition and size (see section 2.1.1). The ISRF has been taken from Mathis, Mezger & Panagia (1983), and has been held fixed for all model runs. The gas component is assumed to be consisting of either (**a**) only hydrogen (section 2.2.1); or (**b**) typical HII region abundance as listed by Ferland (1996) (section 2.2.2). In the latter case, only elements with abundance (relative to hydrogen) higher than 3.0×10^{-6} have been considered. In some model runs for a specific HII region, the elemental abundances used by earlier worker/(s) have been used for comparison. Although the elemental abundance is the same throughout the cloud, the ionization structure and the various level populations depend on several physical parameters including the local radiation field.

The following parameters are explored in order to get an acceptable fit to all the data:

(i) geometric details like $R_{\rm max}$ and $R_{\rm min}$ ($R_{\rm min}$ will not violate radiative destruction of grains);
(ii) radial density distribution law (only three power laws have been explored, viz., $n(r) \approx r^{0}, r^{-1}$ or r^{-2});
(iii) total radial optical depth due to the dust (inclusive of all constituents) at any selected wavelength;
(iv) the dust composition or relative fractions of different constituent grain types (see section 2.1.1).

The interstellar cloud is divided into 141 radial grid points. Near both the boundaries, these grid points are logarithmically spaced (in the rest of the cloud, a linear grid

has been used). The frequency grid consists of 89 points covering the wavelength range 944 A to 5000 μm.

2.1 *Radiative transport through the dust component (D1)*

The radiative transport through the dust component has been carried out by using a programme based on the code CSDUST3 (Egan, Leung & Spagna 1988). We have improvised this code by generalizing the boundary conditions leading to much better flexibility for modelling typical astrophysical sources. The moment equation of radiation transport and the equation of energy balance are solved simultaneously as a two-point boundary value problem in this programme. The effects of multiple scattering, absorption and re-emission of photons on the temperature of dust grains and the internal radiation field have been considered. In addition, the following details, viz., the radiation field anisotropy, linear anisotropic scattering and multi grain components are also included. The entire relevant spectral range covering right from the UV wavelengths to the millimeter region has been considered (the frequency grid consists of 89 points).

For preserving the energetics precisely and self-consistently, the total energy available for heating of the dust component includes all three components (all components being binned into the respectively relevant spectral grid elements):

(i) the star cluster/ZAMS stellar luminosity in photons below the Lyman limit ($\lambda > 912$ Å);
(ii) a part of the Lyman continuum luminosity of the embedded star, ($\lambda < 912$ Å), directly absorbed by the dust; and
(iii) a fraction of the same reprocessed by the gas.

The last contribution, viz., the reprocessed Lyman continuum photons, has been quantified by the prescription of Aller & Liller (1968) that each Lyman continuum photon emitted by the star ultimately leads to one Ly-α photon and one Balmer-α photon.

From the resulting dust temperature distribution in the cloud, the emergent intensities as a function of frequency at various impact parameters (depending on the radial grid) are calculated. Hereafter, the above modelling scheme is referred to as “D1”.

2.1.1 *Dust grains*

Two different approaches have been taken to deal with the dust grains in the present study. The first approach, referred to as “DL” (since largely based on grain properties of Draine & Lee (1984)), is summarized below. The physical properties of the grains, viz., absorption and scattering efficiencies, $Q_{abs}(a,v)$,$Q_{sca}(a,v)$, and the scattering anisotropy factor, $g(a, v)$, for all sizes (a) and frequencies (v) have been taken from the tables of B.T. Draine’s home page which are computed similar to Laor & Draine (1993). These have a finer grid of grain sizes than Draine & Lee (1984). Three types of most commonly accepted variety of interstellar dust have been included in this DL case, viz., (**i**) Graphite, (**ii**) Astronomical Silicate and (**iii**) Silicon Carbide (SiC). The relative abundances of these three types of grains are used as parameters to fit the observed SED well.

In the second approach, the dust grain properties proposed by Mezger, Mathis & Panagia (1982) have been used. This approach, hereafter "MMP", has been considered since it has been found very useful in explaining the SED of certain class of YSO's (Butner *et al.* 1994). This type of dust consists of graphite and silicate only, but their absorptive and scattering properties differ substantially from those for the DL case.

The size distribution of the dust grains is assumed in accordance with Mathis, Rumpl & Nordsieck (1977), to be a power law, viz., $n(a)\mathrm{d}a \sim a^{-m}\mathrm{d}a$, $a_{min} \leq a \leq a_{max}$ with $m = 3.5$. The lower and upper limits of the grain size distribution a_{min} and $a_{\max}$ have been chosen as recommended by Mathis, Mezger & Panagia (1983), to be 0.01 μm and 0.25 μm respectively.

2.2 *Radiative transport through the gas component*

Two independent approaches have been taken to deal with the radiative transfer through the gas component in spherical geometry. The first one takes a very simplistic view considering photoionization and recombination of hydrogen alone, neglecting other heavier elements, as well as the gas-dust coupling (where they co-exist). The treatment of this first approach has been entirely developed in the present study.

The second approach is more sophisticated and considers several prominent elements in the gas phase of the cloud. In addition to photoionization and recombination, other physical processes like collisional excitation and de-excitation, grain photoionization and gas-dust coupling are also included. This detailed modeling involves the use of the photoionization code CLOUDY (Ferland 1996), which has been supplemented with a software scheme developed in the present work, to make the model predictions more realistic and easy to compare with observations.

Whereas the first approach has been used to compute the expected radio continuum emission (without any assumption about optical thinness of the gas at radio wavelength), the second one is used for predicting the atomic/ionic nebular line emission strengths. Both these approaches are discussed next.

2.2.1 *The simple approach (G1)*

In the simple approach, since only hydrogen has been considered, the ionization structure of the gas can be specified by, R_{HII} , the location of the boundary of the HII region (see figure 1). R_{HII} has been determined by considering the radiative transfer of Lyman continuum photons from the embedded star cluster/ZAMS star through the cloud. The effect of the dust component in extinguishing the radiation field, has been considered whenever necessary (cases satisfying $R_{\min} < R_{\mathrm{HII}} < R_{\max}$). In addition, the radio continuum emission has been computed including the effect of appropriate radio optical depth (self absorption). Emission of relevant recombination lines from the ionized gas has been quantified for their role in the radiative transfer through the dust component. Hereafter, this simplistic modelling of the radiative transfer of UV and radio through the interstellar cloud will be referred to as "G1". Appendix 1 gives more details of this treatment.

2.2.2 *The detailed approach (G2)*

For the detailed approach to the radiative transfer through the gas component, the code CLOUDY (Ferland 1996), supplemented by a software scheme developed in the

present study, has been used. The supplementary scheme improves the modelling by (i) emulating the exact structure of the compact HII region; and (ii) including the absorption effects of the dust (present within the line emitting zones), on the emergent line intensities. This detailed approach self-consistently deals with almost all physical processes (radiative-collisional equilibrium) important in and around a photoionized nebula. It simultaneously looks for statistical and thermal equilibrium by solving the equations balancing ionization-neutralization processes and heating-cooling processes. It predicts physical conditions of the gas, e.g., ionization, level populations, temperature structure, and the emerging emission line spectrum. The gas component of the cloud has been considered with typical HII region abundance, as tabulated in Ferland (1996). This is an average of Baldwin *et al.* 1991, Osterbrock, Tran & Veilluex 1992, and Rubin *et al.* 1991, unless specified otherwise. Only the elements with abundance relative to hydrogen, higher than 3.0×10^{-6} have been used. This results into the following elements: H, He, C, N, O, Ne, Mg, Si, S and Ar. The grains of the Astronomical Silicate and Graphite types have been introduced at and beyond a radial distance from the exciting star such that they do not heat up above their sublimation temperature. The heating (photoelectric) and cooling (collisional) due to grains have been considered. The effect of a constant cosmic ray density on the gas is included (which affects energy deposition and ionization).

To be self-consistent with the radiative transfer treatment through the dust component (D1), the entire cloud is considered to be consisting of two spherical shells, the inner one made of gas alone and the outer one with gas and dust. The boundary between the two shells, $R_{\rm min}$, is taken from the corresponding best fit D1(DL) or D1(MMP) model. CLOUDY is run twice, the first time (RUN1) for the inner pure gas shell with the central energy source. The continuum emerging from RUN1 is used as input to the second run (RUN2) for the outer shell. The emerging line spectrum from RUN1 is transported to an outside observer, through the second (outer) shell by considering the extinction due to the entire dust column present there. For every spectral line considered, its emissivities from individual radial zones of RUN2 are transported through the corresponding remaining dust column densities within the outer shell. The emerging line luminosities from RUN1 and RUN2 are finally added to predict the total observable luminosity. This detailed modelling scheme will be referred to as "G2" in the later text.

A total of 27 most prominent spectral lines (from various ionization stages of the above mentioned 10 elements) have been considered. From an observational point of view, the reliable detectability of any spectral line will depend on experimental detail like: the instrument line function (spectral resolution); as well as the strength of the continuum in the immediate spectral neighbourhood of the line. An attempt has been made to predict line intensities for those lines which are detectable by the spectrometers onboard ISO (SWS & LWS).

A line has been defined to be "detectable" only if the expected power incident on the detector, due to the spectral line is more than 1% of the continuum (from the same astrophysical source, originating from the dust) in the corresponding resolution element. An instrumental resolution in the range 1000–20000 has been reported for ISO spectrometers depending on the wavelength (de Graauw *et al.* 1996; Swinyard *et al.* 1996). The lines are in general narrower than the resolution element if the widths are thermal. Only the lines turning out to be "detectable" according to the above criteria are presented with details.

3. Study of the galactic star forming regions: IRAS 183140720, 183550532 and 183160602

With the aim of extracting important geometrical and physical details of the galactic star forming regions—IRAS 18314–0720, 18355–0532 and 18316–0602, the modelling scheme described earlier, has been applied. These sources have been selected to cover a range of ≈ 40 in the total luminosity. In addition, they have adequate observational data necessary to constrain the modelling. In what follows, the observations available for these sources and the results of modelling them, are described.

3.1 *IRAS 18314–0720*

The IRAS Point Source Catalog (hereafter, IRAS PSC) source 18314–0720 has flux densities of 156, 648, 4714 and 8089 Jansky in 12, 25, 60 and 100 μm bands respectively. Although this source did not appear in the original IRAS Low Resolution Spectra Atlas (8–22 μm; hereafter LRS), later analysis released the LRS spectrum of this source (Volk & Cohen 1989). Based on the LRS spectrum, forbidden lines of ions of neon and sulphur have been identified as well as possible detection of features due to Polycyclic Aromatic Hydrocarbons have been reported (Jourdain de Muizon *et al.* 1990). Recently, mid and far infrared spectroscopic detection of several ionic lines based on Kuiper Airborne Observatory measurements have become available (Afflerbach *et al.* 1997). IRAS 18314–0720 corresponds to the Revised Air Force Geophysical Laboratory source RAFGL 2190, which was detected in 4.2, 11, 20 and 27 μm bands. IRAS 18314–0720 was included in the IRAS colour selected sample of Chini *et al.* (1986) for study at 1.3 mm continuum and near infrared mapping (Chini *et al.* 1987), Bronfman *et al.* (1996) have detected *CS* emission at 98 GHz from IRAS 18314–0720. In a search for NH_3 and H_2O maser sources associated with this source, the former has been detected but not the latter (Churchwell *et al.* 1990).

The radio continuum emission from the HII region associated with IRAS 18314–0720 has been observed at various frequencies. The IRAS PSC associates 18314–0720 with radio continuum sources of Parkes and Bonn surveys of the Galactic plane at 5 GHz (Haynes *et al* 1979; Altenhoff *et al* 1979). Later surveys, some with higher angular resolution at 1.4, 5 and 10 GHz have detected this source (Handa *et al.* 1987; Becker *et al.* 1994; Griffith *et al.* 1995; Zoonematkermani *et al.* 1990). It has also been mapped with high angular resolution at 1.5, 4.9 and 15 GHz (Garay *et al.* 1993).

3.1.1 *Observational constraints*

Among all available observational data for IRAS 18314–0720, those most relevant for constraining the modelling are chosen based on their quality/sensitivity and the beam size (a smaller beam size is preferred since we are dealing with compact HII regions which are barely resolved in mid and far infrared wavebands). These include: IRAS PSC, LRS, 1.3 millimeter and the near infrared data for constructing the continuum SED. Observations at wavelengths longer than 1.3 mm have not been used to constrain the models because at these wavelengths the free-free emission from the gas will be a major contributor. Hence in order to compare with the dust continuum emission predicted by the models, one would need to subtract out the estimated free-free emission from the measurements. From the observations at 7 mm (Wood *et al.*

1988) it is clear that, the contamination due to the free-free emission is negligible at 1.3 mm. The infrared forbidden line measurements of ions though detected in LRS, they are only qualitative in nature, hence the only quantitative data from the Kuiper Observatory has been used in the present study. The distance to this source has been taken to be 9.4 kpc from Chan *et al.* (1996). Accordingly the total luminosity (from the observed SED) turns out to be $1.02 \times 10^6\ L_{\odot}$. The radio continuum measurements at 5 GHz (VLA) and 10 GHz (Nobeyama) by Garay *et al.* (1993) and Handa *et al.* (1987) respectively, have been used for model fitting.

3.1.2 *Results of modelling*

With the above observational constraints, the spherically symmetric radiative transfer model D1 has been run (with both DL and MMP type of dust) exploring various parameters described earlier.

The resulting best fit model for the DL dust case, corresponds to:

(i) a single ZAMS star of type 04 ($T_{\rm eff}$ = 50,000 K) as the embedded source;
(ii) a uniform density distribution (i.e. $n(r) = n_0$);
(iii) the radial optical depth at 100μm, $\tau_{100} = 0.1$;
(iv) the gas to dust ratio by mass, 100:1;
(v) the density $n_H = 1.15 \times 10^4 \rm cm^{-3}$;
(vi) $R_{\rm max}$ = 2.5pc;
(vii) $R_{\rm min}$ = 0.05 pc; and
(viii) the dust composition,silicate: graphite: silicon carbide in 7.2:45.3:47.5% proportion.

This D1(DL) model predictions fit the observed SED extremely well, which is shown in Fig. 2. The predicted radio continuum emission at 5 GHz (determined by G1(DL) ran), using these parameters, is only 324 mJy which is almost one tenth of the observed value of 3.51 Jy. The increase in the gas to dust ratio needed to bring the radio continuum emission close to the observed value would be very unphysical. The total cloud mass for this model turns out to be $1.85 \times 10^4 M_{\odot}$ implying the *L/M* ratio to be 55 ($L_{\odot}/M_{\odot}$).

On the other hand, the MMP dust case leads to the following best fit parameters:

(i) a single ZAMS star of type O4 ($T_{\rm eff}$ = 50,000K) as the embedded source;
(ii) a uniform density distribution (i.e. $n(r) = n_0$);
(iii) the radial optical depth at 100 μm, $\tau_{100} = 0.1$;
(iv) the gas to dust ratio by mass, 300:1;
(v) the density $n_H = 3.76 \times 10^4\ \rm cm^{-3}$;
(vi) $R_{\rm max}$ = 2.5 pc; (vii) $R_{\rm min}$ = 0.05 pc; and
(viii) the dust composition, silicate: graphite in 11.5 : 88.5% proportion.

The fit to the observed SED for this D1(MMP) model is also shown in Fig. 2. Although the fit is reasonably acceptable, the absorption feature at ≈ 10 μm predicted by this model is much narrower than the LRS measurements. However, the predictions for radio emission at 5 and 10 GHz in this case (G1(MMP)), viz., 3.56 Jy and 4.56 Jy respectively, match the observations very closely (3.51 Jy and 4.51 Jy). The total cloud mass in this case, turns out to be $5.78 \times 10^4 M_{\odot}$ implying an *L/M* ratio of 17.3 ($L_{\odot}/M_{\odot}$).

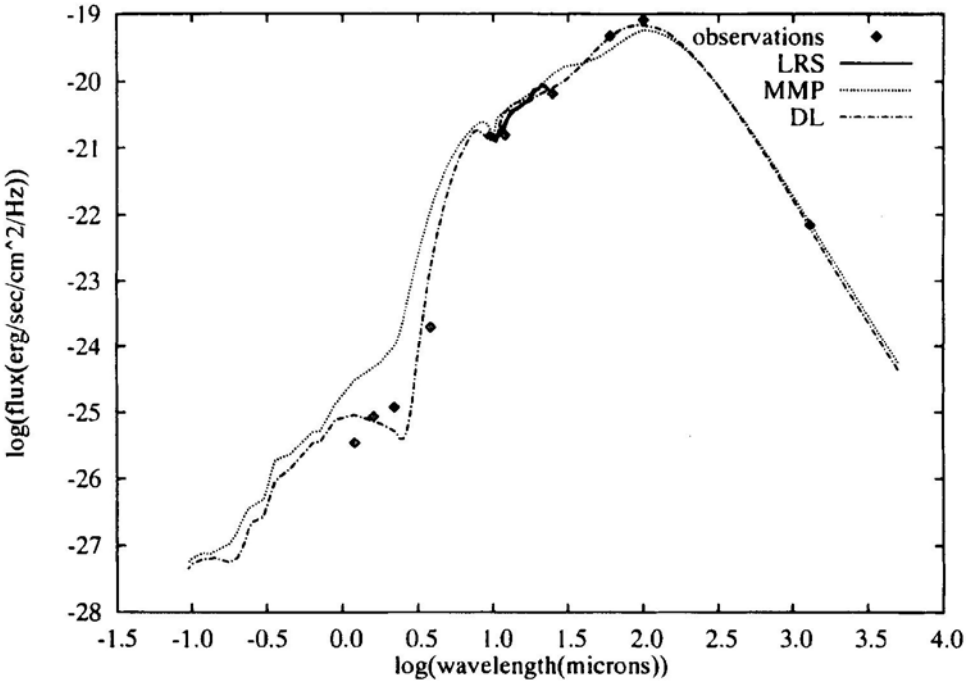

Figure 2. Spectral energy distribution for the source IRAS 18314–0720; the solid line represents LRS observations; the dashed line represents model with MMP grains; the dash-dot-dash line represents model with DL grains; and the symbol ◊ represents other observations (see text).

A comparison between the best fit parameters with DL and MMP dust, constrained by the observations of IRAS 18314–0720, bring out the following: most of the important parameters are identical including even the radial optical depth. This is quite reassuring to note that the geometry as well as the radial density distribution law are invariant to the type of dust (among DL and MMP) selected. Major differences exist for the radio continuum emission predicted and the dust grain composition. Considering the overall fit to the observed continuum SED from the dust and the radio continuum emission from the gas component, clearly the MMP is the favoured self-consistent model for IRAS 18314–0720. Next, we consider the additional information from the forbidden line emission of ionized heavy elements.

In order to predict the forbidden line emission from various ionized species of the gas component in IRAS 18314–0720, the G2 model calculations have been carried out. Runs have been made with the best fit parameters for both the models D1(DL) and D1(MMP). The resulting line luminosities are presented in Table 1. As described above (section 2.2.2) among the 27 relevant lines, only those are included which have intensities more that 1% of the neighbouring continua (for assumed instrumental spectral resolutions of the ISO spectrometers). The observed line strengths of IRAS 18314–0720, for the [SIII] (18.7 μm), [OIII] (51.8 and 88.4μm), and [NIII] (57.3 μm) lines as reported by Afflerbach *et al.* (1997; ACW), are listed in Table 2. The corresponding model predictions (in identical units) for both G2(DL) and G2(MMP) cases are presented in Table 2 for comparison. It is clear that both the models predict far less line emission (for all the four lines) compared to the observations. However, the DL

Table 1. Luminosities of detectable lines from the three sources predicted from their models.

Line (wavelength in μm)	IRAS 18314–0720		IRAS 18355–0532		IRAS 18316–0602	
	DL	MMP	DL	MMP	DL	MMP
	$L_\odot$	$L_\odot$	$L_\odot$	$L_\odot$	$L_\odot$	$L_\odot$
CII (157.7)	2.50	2.93	0.53	0.62	0.15	0.14
OI (145.6)	0.45	3.00	0.14	0.70	0.05	0.13
NI (121.8)	0.09	0.05	0.01	0.01	0.002	0.001
OIII (88.4)	31.3	28.75	1.62	1.76	–	–
OI (63.2)	2.60	4.90	0.88	1.14	0.02	0.20
NIII (57.2)	13.8	10.42	1.07	0.86	–	–
OIII (51.8)	179.3	109.5	10.3	7.18	–	–
NeIII (36.0)	19.3	10.18	1.37	0.72	–	–
SiII (34.8)	0.66	0.46	0.11	0.13	0.03	0.02
SIII (33.5)	10.9	1.73	1.05	0.22	0.03	–
OIV (25.9)	18.9	0.53	0.11	–	–	–
ArIII (21.8)	1.24	–	0.16	–	–	–
SIII (18.7)	19.6	0.48	2.38	0.07	0.06	–
NeIII (15.6)	124.8	15.55	9.70	1.37	–	–
ArV (13.1)	0.70	–	–	–	–	–
NeII (12.8)	1.37	–	0.64	0.12	0.17	0.006
ArIII (10.5)	18.9	–	0.75	–	–	–

Table 2. Comparison of model predictions and observed line intensities (Afflerbach *et al.* 1997) of IRAS 183140720.

Line (wavelength in μm)	Line intensities (10^{-18} watts cm^{-2})			
	G2(DL)	G2(MMP)	Observations (ACW)	G2(ACW)
SIII (18.7)	0.74	0.02	53.0 ± 4.2	47.00
OIII (51.8)	6.78	4.14	51.9 ± 3.8	80.21
NIII (57.2)	0.52	0.39	32.9 ± 2.4	16.55
OIII (88.4)	1.18	1.09	22.3 ± 1.6	26.67

case fares relatively better than the MMP case. ACW have explained these line emissions, originating from a region with electron density n_e = 825 cm^{-3} and $T_{\rm eff}$ = 35, 000 K. Their n_e is too low compared to our models. Perhaps that is the main reason for the discrepancy. In order to verify that, another G2 run is carried out, with the values of n_e, $T_{\rm eff}$ and the elemental abundances identical to those of ACW, but all other details identical to our D1(MMP) model. Results of this run, G2(ACW), are also presented in Table 2. The G2(ACW) predictions are very close to the observations for the [SIII] (18.7 μm) and [OIII] (88.4 μm) lines and within a factor of two for the rest.

This confirms that a lower value of n_e is mainly responsible for the higher observed line intensities in general. This is not unexpected since the collisional de-excitations will become important at higher densities thereby reducing the probability of radiative decays.

The above implies that although a uniform density self-consistent picture is able to explain the SED from the dust and the radio continuum emission from the gas, it fails to explain details of fine structure line strengths for ionized heavy elements. Whereas

the former suggests higher densities, the latter favours a lower one. The detection of molecular maser sources and CS line emission give additional support to the existence of dense medium predicted by our models. In actual source, the reality may lie somewhere in between, viz., a mixture of dense clumps in a thinner inter-clump medium. We explore the role of clumpiness on resolving the issue of fine structure line strengths. Consider the following simplistic scenario: clumps of constant density (ρ_1) immersed in the inter-clump (lower density of ρ_2) medium, with a volume filling factor of f . The clumps are of uniform size and are uniformly distributed throughout the interstellar cloud. This picture has three parameters, viz., ρ_1 , ρ_2 and f.

In this approach, the inter-clump medium (with density p_2, as in the model of ACW) will be mainly responsible for the fine structure line emission (collisional deexcitation will be more important in the clumps). On the other hand, the radio continuum emission will be dominated by the region with higher n_e^2, i.e. the clumps. In addition, if the fit to the observed continuum emission from the dust (SED) is to remain intact, the effective total optical depth (due to dust grains) has to match that from the radiative transfer model (DL or MMP). Hence, there are three constraints to the scenario of clumpy medium: ρ_2 dictated by the fine structure line data;$\langle n_e^2 \rangle$ from the radio continuum; and the dust optical depth from the continuum SED.

Assuming both the clump and the inter-clump medium to be optically thin in the radio; using the above three constraints; and DL type dust; we obtain the following parameters for IRAS 18314–0720. The clumps with a density of 1.34×10^5 cm^{-3} are embedded in the inter-clump medium (with a density of 825 cm^{-3}; same as in ACW), with a volume filling factor of 0.08. The detection of 98 GHz line from the CS molecule, whose excitation requires a critical density $\approx$ 3–4$\times 10^5$ cm^{-3}, further supports the above density of the clumps.

For the radiative transfer modelling of the continuum SED to remain valid, the individual clumps must be optically thin even at the lowest relevant wavelength (i.e. UV). This condition translates the clump diameter to be less than 10^{-3} parsec. For this size, the clumps are found to be optically thin at radio wavelengths as well, thus justifying our assumption of the same in calculating the density (ρ_1) and the volume filling factor of the clumps.

Thus, a self-consistent picture of IRAS 18314–0720 emerges with the DL model including clumpiness, which explains all three major types of observational constraints, viz., continuum SED, radio continuum and fine structure line emission from ionized heavy elements.

3.2 *IRAS 18355–0532*

The IRAS PSC source 18355–0532 has flux densities of 24.6, 209, 1127 and 1930 Jy in 12, 25, 60 and 100 μm bands respectively. This source is included in the original IRAS LRS Catalog. An inspection of the LRS spectrum led to the identification/possible identification of forbidden lines of neon and sulphur ions (Jourdain de Muizon *et al.* 1990). More detailed analysis has identified and quantified emission in a total of four lines from neon and sulphur (Simpson & Rubin 1990). IRAS 18355–0532 corresponds to the RAFGL catalogue source no. 2211, which was detected in 4.2, 11 and 20 μm bands. IRAS 18355–0532 was also included in the IRAS colour selected sample of Chini *et al.* (1986) for study at 1.3 mm continuum and near infrared mapping (Chini *et al.* 1987). Although the CS emission at 98 GHz has been detected

from IRAS 18355–0532 (Bronfman *et al.* 1996), the searches for H_2O (22.2 GHz) and methanol (6.6 GHz) maser emission have been unsuccessful (Codella *et al.* 1995; Schutte *et al.* 1993).

The radio continuum emission associated with IRAS 18355–0532 has been observed at various frequencies. The IRAS PSC associates 18355–0532 with radio continuum sources of Parkes and Bonn surveys of the Galactic plane at 5 GHz (Haynes *et al.* 1979, Altenhoff *et al.* 1979). Later surveys have also detected this source at 1.4, 5 and 10 GHz (Handa *et al.* 1987; Becker *et al.* 1994; Griffith *et al.* 1995; Zoonematkermani *et al.* 1990).

3.2.1 *Observational constraints*

The observations of IRAS 18355–0532 have been chosen to constrain its modeling in the same fashion as in the case of IRAS 18314–0720. The observed SED has been constructed by the following measurements: IRAS PSC, IRAS LRS, 1.3 millimeter and the near infrared data. The infrared forbidden line intensities have been taken from Simpson & Rubin (1990), who have analysed and quantified the IRAS LRS measurements. The distance adopted to this source has been taken to be 6.6 kpc from Chini *et al.* (1987). The total luminosity of IRAS 18355–0532 from the observed SED is estimated to be $1.21\times10^5 L_{\odot}$. The radio continuum measurements at 5 GHz (VLA; Becker *et al.* 1994) and 10 GHz (Nobeyama; Handa *et al.* 1987) have been used for model fitting.

3.2.2 *Results of modelling*

The best fit parameters for the radiative transfer modelling (D1(DL) case) of IRAS 18355–0532, are as follows:

(i) a single ZAMS star of type 06.5 ($T_{\rm eff}$ = 40,000 K) as the embedded source;
(ii) a uniform density distribution (i.e. $n(r) = n_0$);
(iii) the radial optical depth at 100 μm, $\tau_{100} = 0.1$;
(iv) the gas to dust ratio by mass, 100:1;
(v) the density $n_H = 1.71\times10^4$ cm^{-3};
(vi) $R_{\rm max}$ = 1.3pc;
(vii)$R_{\rm min}$ = 0.007 pc; and
(viii) the dust composition, silicate : graphite : silicon carbide in 6.0:46.4:47.6% proportion.

The fit of this D1(DL) model to the observed SED is shown in Fig. 3. This fit is very good for most of the spectral region, including the 10 μm feature. Although, the model curve passes closely to the 25 μm point of the IRAS PSC, it deviates from the longer wavelength region (≈ 15–22 μm) of the LRS spectrum. The radio continuum emission predicted by this model, at 5 GHz is only 51 mJy which is again one tenth of the observed value of 523 mJy. Like we stated earlier (in the case of IRAS 18314–0720), for IRAS 18355–0532 also, we avoid increasing the gas to dust ratio to bring the radio continuum emission closer to the measurements, since that would require a very unphysical value. The total cloud mass for this model turns out to be $4.93\times10\,M_{\odot}$ implying the L/M ratio to be 24.5 ($L_{\odot}/M_{\odot}$).

The D1 (MMP) modelling leads to be the following best fit parameters for IRAS 18355–0532:

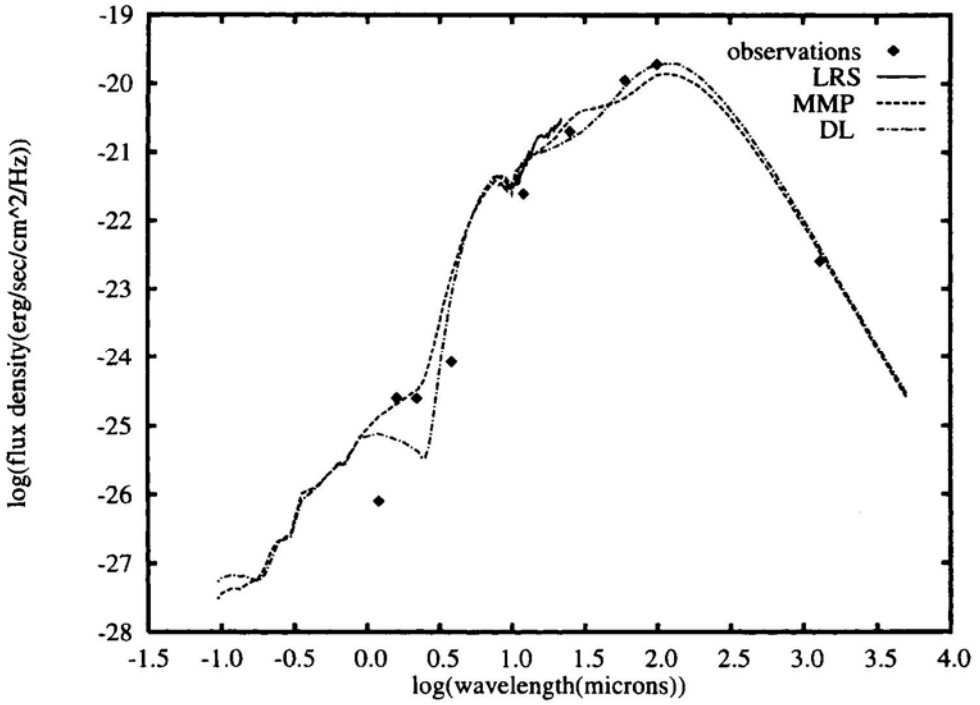

Figure 3. Spectral energy distribution for the source IRAS 18355–0532; the solid line represents LRS observations; the dashed line represents model with MMP grains; the dash-dot-dash line represents model with DL grains; and the symbol ◇ represents other observations (see text).

(i) a single ZAMS star of type 06.5 ($T_{\rm eff}$ = 40,000 K) as the embedded source;
(ii) a uniform density distribution (i.e. $n(r) = n_0$);
(iii) the radial optical depth at 100 μm, $\tau_{100} = 0.1$;
(iv) the gas to dust ratio by mass, 300:1;
(v) the density $n_H = 7.20 \times 10^4$ cm^{-3};
(vi) $R_{\rm max} = 1.3$pc;
(vii) $R_{\rm min} = 0.018$ pc; and
(viii) the dust composition, silicate: graphite in 12: 88% proportion.

The fit to the observed SED for D1(MMP) model is also shown in Fig. 3, which is reasonably good. This model fits the longer wavelength segment of the LRS spectrum quite well (which the DL case could not), but the 10 μm feature predicted is much narrower than the observed one. The fit to 60 and 100 μm IRAS PSC points is slightly poorer than the DL case. This G1(MMP) case is much more successful than G1(DL), in predicting the radio continuum emission. The predicted values for this case (G1(MMP)), are 872 mJy and 1.18 Jy at 5 and 10 GHz respectively, which are very close to the observed numbers (523 mJy and 1.61 Jy). The mass of the cloud associated with IRAS 18355–0532, for the parameters of this MMP model, is $1.56 \times 10^4 L_\odot$. This implies an L/M ratio of 7.8 ($L_\odot/M_\odot$)

Comparing the best fit parameters for IRAS 18355–0532, for the models with DL and MMP dust, one finds conclusions similar to the earlier case of IRAS 18314–0720.

Table 3. Comparison of model predictions and observed line intensities (Simpson & Rubin 1990) of IRAS 18355–0532.

Line (wavelength in μm)	Line intensities (10^{-18} watts cm^{-2})			
	G2(DL)	G2(MMP)	Observations (SR)	G2(SR)
SIV (10.5)	0.058	1.50×10^{-5}	0.5	3.09
NeII (12.8)	0.048	9.037×10^{-3}	14.0	2.55
NeIII (15.6)	0.745	0.105	8.1	6.91
SIII (18.7)	0.182	5.219×10^{-3}	14.0	8.35

Most important parameters are identical, e.g., radial density distribution and the radial optical depth. The differences exist for the predicted radio continuum and the dust grain composition. Once again, the MMP model is the favoured model for IRAS 18355–0532, since it self consistently fits the observed continuum SED as well as the radio continuum emission, reasonably well. Similar to the earlier source, here again we consider the data of fine structure lines of ionized heavy elements in IRAS 18355–0532.

The predictions from the G2 runs for IRAS 18355–0532, corresponding to the above mentioned best fit parameters of D1(DL) as well as D1(MMP) models are also presented in Table 1. Once again the line luminosities for only the detectable infrared forbidden lines are included. Simpson & Rubin (1990; SR) have carefully analysed the 822 μm IRAS LRS data for IRAS 18355–0532, as one member of a large sample. They have quantified the line intensities for [SIV] (10.5 μm), [Nell] (12.8 μm), [NeIII] (15.6 μm) and [SIII] (18.7 μm) lines. These are also presented in Table 3. The corresponding model predictions (in identical units) for both G2(DL) and G2(MMP) cases are listed in Table 3 for easy comparison. Both the models predict far less line emission (for all the four lines) compared to the observations. Just like in the earlier case of IRAS 18314–0720, for IRAS 18355–0532 also, the DL fares much better than the MMR

Since there are two pairs of lines from the same elements, viz., S and Ne, the line ratios will be less sensitive to the abundances. Whereas the measured intensity ratios between [NeII]/[NeIII] and [SIII]/[SIV] are 1.7 and 28 respectively, the same for the G2(DL) model are 0.06 and 3.1. It is interesting to note that, if in the same G2(DL) model, the $T_{\rm eff}$ is reduced to 28,000 K, then both the observed line ratios are reproduced.

SR have modelled the line emissions from IRAS 18355–0532, with electron density $n_e = 3.16 \times 10^3$ and $T_{\rm eff} = 38{,}500$ K. This n_e is very low compared to our models. In addition, their elemental abundances are different from ours. In order to verify the hypothesis that, the high value of n_e is responsible for the failure of our models to predict the line intensities, another G2 run is carried out with the abundances, n_e and $T_{\rm eff}$ values from SR, but all other details same as D1(MMP). Predictions of this model, G2(SR), are also presented in Table 3. The G2(SR) predictions are reasonably close to the observations for the [NeIII] (15.6 μm) and [SIII] (18.7 μm) lines but the other two line intensities are down by a factor of ≈ 6. This success of G2(SR) supports the above hypothesis about the value of n_e, which is not unexpected since the collisional de-excitations become less important at lower densities.

Once again, like in the case of IRAS 18314–0720, for IRAS 18355–0532 also, a uniform density self-consistent picture is able to explain the SED from dust and the

radio continuum emission from the gas, but fails to explain details of fine structure line strengths for ionized heavy elements. The detection of molecular maser sources and CS line further supports the existence of denser medium predicted by our self-consistent models. Since again, a lower value of n_e has been relatively more successful in predicting the forbidden line strengths, we propose the possible scenario of clumpiness in IRAS 18355–0532 too, for resolution of the above problem, like the earlier case of IRAS 18314–0720.

Using an identical approach of incorporating clumpiness in IRAS 18355–0532, as was used for the earlier source IRAS 18314–0720, a physically meaningful solution has been found corresponding to the DL scheme of modelling. This solution corresponds to the following parameters: $\rho_1 = 2.12 \times 10^5$ cm^{-3}; $\rho_2 = 3.16 \times 10^3$ cm^{-3} (same as in SR) and $f = 0.067$. The detection of 98 GHz line from the CS molecule further supports the above density inside the clumps. Once again, arguing from the point of validity of the DL modelling of the continuum SED, the upper limit on the diameter of the clumps is set to 5.2×10^{-4} parsec.

Thus, even for IRAS 18355–0532, a self-consistent picture emerges with the DL model including clumpiness, which explains all three major types of observational constraints.

3.3 *IRAS 18316–0602*

The IRAS PSC source 18316–0602 has flux densities of 22.8, 138, 958 and 2136 Jansky in 12, 25, 60 and 100 μm bands respectively. This source is included in the IRAS LRS Catalog. The LRS spectrum shows the 10 μm silicate feature, but no forbidden line or any feature due to the Polycyclic Aromatic Hydrocarbons (Jourdain de Muizon *et al.* 1990). However, recent ISO-SWS measurements of IRAS 18316–0602 do show a very rich spectrum full of various solid state molecular features (d'Hendecourt *et al.* 1996; Dartois *et al.* 1998). IRAS PSC associates 18316–0602 with RAFGL 7009S, which was detected at 4.2, 11, 20 and 27 μm. Sub-millimeter and millimeter waveband continuum observations of IRAS 18316–0602 have been carried out at 450, 800, 850 and 1100 μm by Jenness *et al.* (1995) and McCutcheon *et al.* (1995). The 2.6 mm CO line has also been detected from this source by McCutcheon *et al.* 1991. The CS and NH_3 emission have been detected from IRAS 18316–0602 (Bronfman *et al* 1996; Molinari *et al.* 1996). Searches for H_2O and methanol maser emission from this source have also been successful (Brand *et al.* 1994; van der Walt *et al.* 1995; Codella *et al.* 1996)

The radio continuum emission associated with IRAS 18316–0602 has been observed at 5 and 8 GHz (Jenness *et al.* 1995; McCutcheon *et al* 1991; Kurtz *et al.* 1994; Griffith *et al.* 1995).

3.3.1 *Observational constraints*

The observed SED for IRAS 18316–0602 has been generated from the following: IRAS PSC, IRAS LRS, selected continua from the ISO-SWS spectrum (3–8 μm) and all theavailable sub-mm/mm observations (450–1100 μm).Radio continuum data at 5 and 8 GHz have been used as constraints for the modelling of this source.

The distance to this source has been taken to be 3.3 kpc from Chan *et al.* (1996). The corresponding total luminosity is $2.54 \times 10^4 L_\odot$.

3.3.2 *Results of modelling*

The total luminosity of IRAS 18316–0602 corresponds to a single ZAMS star of type BO ($T_{\rm eff}$ = 30,900 K). However, since a single ZAMS star as the embedded source leads to a poor fit to the observed SED as well as the radio continuum data, various clusters of ZAMS stars with a given Initial Mass Function but a variable upper mass cut-off (M_u), have been tried. After exploring the parameter space for Dl(DL) modelling, the following best fit parameters have been determined for IRAS 18355–0532:

(i) a cluster of ZAMS stars with an Initial Mass Function of the form $N\ (M) \approx M^{-2.4}$, with the upper mass cut off, M_u, corresponding to the type B1,
(ii) a uniform density distribution (i.e. $n(r) = n_0$);
(iii) the radial optical depth at 100 μm, $\tau_{100} = 0.1$;
(iv) the gas to dust ratio by mass, 100:1;
(v) the density $n_H = 2.28 \times 10^4$ cm^{-3};
(vi) $R_{\rm min} = 0.0001$ pc; and
(vii) the dust composition, silicate: graphite: silicon carbide in 71.8:28.2:0.0% proportion.

The above parameters are also consistent with the column density (N_{H_2}) derived from CO measurements of McCutcheon *et al* 1991. The fit of this D1(DL) model to the observed SED is shown in Fig. 4. This fit is very good for most of the spectral

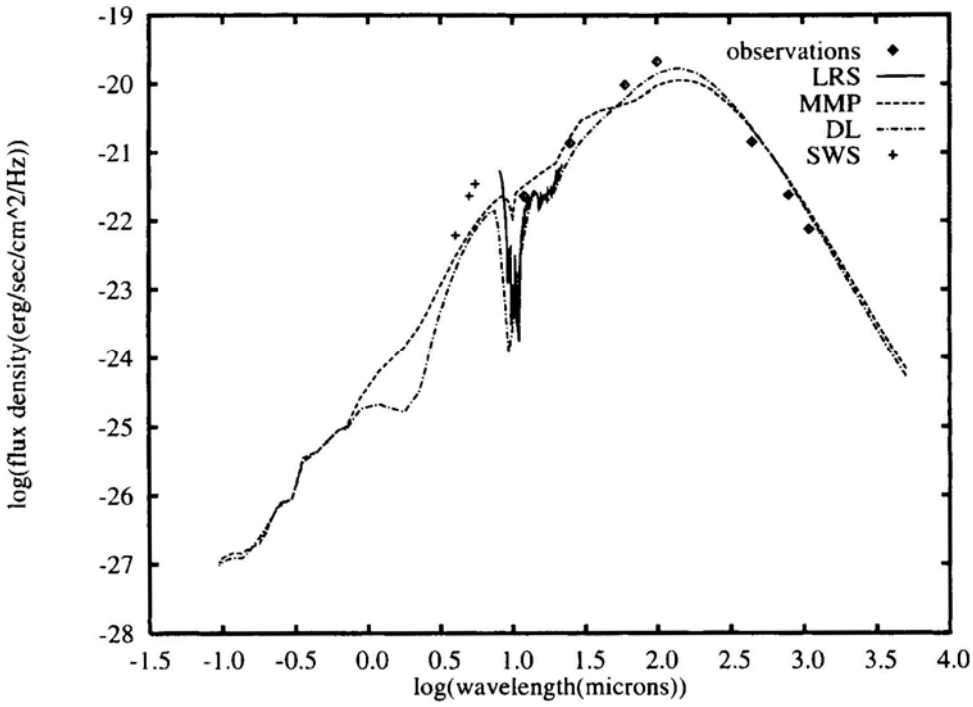

Figure 4. Spectral energy distribution for the source IRAS 18316–0602; the solid line represents LRS observations; the dashed line represents model with MMP grains; the dash-dot-dash line represents model with DL grains; the symbol + represents SWS observations; and the symbol ◇ represents other observations (see text).

region, particularly for the longer wavelengths of the LRS spectrum. The position of the predicted ≈ 10 μm feature is slightly to the shorter wavelength side compared to the observations (LRS). Any attempt to "align" this feature towards the longer wavelength by increasing SiC dust relative to the silicate dust, leads to very poor fit to the 15–22 μm part of the spectrum (LRS data). Incidentally, the SiC dominant dust composition corresponding to the best aligned feature, is – silicate: graphite: silicon carbide in 0.9:11.0: 88.1% proportion. Although the predicted SED by the DL model passes acceptably close to the ISO-SWS continuum at 4.0 μm, the fit is rather poor at 5.0 and 5.5 μm, the observed values being about 3 times the predictions. The radio continuum emission predicted corresponding to this model, at 5 GHz is about 2.16 mJy which is reasonably close to the observed value of 2.7 mJy. In fact a slight increase the gas to dust ratio can bring the model prediction exactly to the measured value the total cloud mass for this DL model turn out to be 3.88×10^3 $M_\odot$ implying the L/M ratio to be 6.55 ($L_\odot/M_\odot$).

The D1(MMP) modelling leads to the following best fit parameters for IRAS 18316–0602:

(i) a cluster of ZAMS stars with an Initial Mass Function of the form $N(M) \approx M^{-2.4}$, with the upper mass cut off, M_u, corresponding to the type B1
(ii) a uniform density distribution (i.e. $n(r) = n_0$);
(iii) the radial optical depth at 100 μm, $\tau_{100} = 0.1$;
(iv) the gas to dust ratio by mass, 300:1;
(v) the density $n_H = 7.74 \times 10^4 \mathrm{cm}^{-3}$;
(vi) $R_{\min} = 0.0005$ pc; and
(vii) the dust composition, silicate: graphite in 11: 89% proportion.

The fit to the observed SED of IRAS 18316–0602 by the D1(MMP) model is also shown in Fig. 4. Although this fit crudely represents the broad overall shape of the SED, it fails to reproduce many details, particularly near the ≈ 10 μm feature. The predicted feature in this MMP case is far too narrow as well as shallow compared to the LRS data. At far infrared wavelengths also (IRAS PSC 60 and 100 μm) the predictions are below the observations. The predicted radio emission at 5 and 8 GHz in this case (G1(MMP)) are 3.3 and 3.4 mJy respectively, which are in reasonable agreement with the observations (2.7 and 3.8 mJy; McCutcheon *et al.* 1991; Jenness *et al.* 1995). The cloud mass for this MMP case is 1.31×10^4 $L_\odot$, leading to a value for the L/M ratio of 1.9 ($L_\odot/M_\odot$).

The D1(DL) is clearly the preferred model for IRAS 18316–0602. The detection of maser sources associated with IRAS 18316–0602 is consistent with best fit model gas densities.

The model G2 prediction (corresponding to the best fit parameters of D1(DL) as well as D1(MMP) cases) for all the detectable infrared forbidden line emission from IRAS 18316–0602 have been presented in Table 1, alongwith other two sources. Although IRAS 18316–0602 has been studied by the ISO-SWS spectrometer covering the entire wavelength range of 2.5–45 μm, the observations/data binning have been carried out at a low resolution of 300–500 (d'Hendecourt *et al.* 1996; Dartois *et al.* 1998). The few selected narrow wavelength regions covered at higher resolution (1500–2000; Dartois *et al.* 1998) do not cover the lines predicted to be detectable by our models (see Table 1). In addition, the detectability criterion used by us uses ISO-SWS observation modes with much higher resolution (in the 12–45 μm

region) than these reported spectra (i.e. even if the predicted lines were covered, they would not have been detectable at this intermediate resolution observational mode employed by Dartois *et al.* 1998).

For IRAS 18316–0602 too, like in the cases of IRAS 18314–0720 and 18355–0532, a uniform density self-consistent picture is able to explain the SED from dust and the radio continuum emission from the gas. Unfortunately, no measurement exists to date, for any infrared fine structure line for this source. In case, IRAS 18316–0602 has been observed using the ISO-LWS spectrometer (in high resolution configuration), then our models can be qualified further.

4. Conclusions

A simple yet self-consistent approach towards explaining observed spectral energy distribution of interstellar clouds with embedded YSO's/compact HII regions has been described. The radiation of the embedded source/(s) is transported through the dust and the gas components by different schemes in spherical geometry. Two kinds of dust have been considered (Draine & Lee (DL); and Mezger, Mathis & Panagia (MMP)), each with its own variable composition. Here, by self-consistent one means that the same geometric and physical configuration fits the observed data for the emission from the dust (most of the infrared, sub-mm, mm part of the SED) as well as the emission from the gas (radio continuum).

The effectiveness of this scheme has been assessed by applying it to three Galactic star forming regions associated with IRAS 18314–0720, 18355–0532 and 18316–0602. They cover a range of about 40 in luminosity of the embedded source/(s). Relevant observational data for these sources have been modelled to extract information about their physical size, density distribution law, total optical depth and dust composition. Interestingly, in all these three cases, the best fit models correspond to the uniform density distribution (for either DL or MMP dust). Similar conclusion about constant density envelopes, has been drawn recently by Faison *et al.* (1998) for a sample of 10 Galactic compact HII regions.

For both IRAS 18314–0720 and 18355–0532, the MMP dust models are the favoured models, since they not only give reasonably acceptable fits to the continuum SED, but also explain the radio continuum data.

Even though SED and radio continuum observations have been well explained by the above modelling, they predict much lower intensities for fine structure lines of ionized heavy elements, wherever measurements are available (IRAS 18314–0720 and 18355–0532). This discrepancy has been resolved by invoking clumpiness in the interstellar medium. Two phase (clump/inter-clump) models with DL type dust, have been successfully constructed for IRAS 18314–0720 and 18355–0532.

In the case of IRAS 18316–0602, DL is the preferred model which gives a very good fit to the observed SED, as well as predicts radio continuum emission which is consistent with the measurements.

Acknowledgements

It is a pleasure to thank Gary Ferland for his help on several occasions regarding the code CLOUDY; and D. Narasimha for clarifying certain doubts about radiative

transfer. Members of Infrared Astronomy Group are thanked for their comments. The authors thank the anonymous referee for the comments which improved the conclusions regarding clumpiness.

APPENDIX 1

A.1 *Simple approach to radiative transfer through the gas (G1)*

In this simple approach, the extent of the ionized region (in spherical geometry) is determined by transporting the Lyman continuum photons (from the centrally located star/star cluster) through the cloud including the effect of the dust, where they can exist (as determined by their sublimation). The gas component of the cloud is assumed to consist of only hydrogen. Next, the radio continuum emission emerging from the cloud is calculated by transporting the radio photons (free-free emission throughout the ionized medium of the cloud), through the entire cloud without making any approximation about the optical thinness of the gas (i.e. self absorption is treated appropriately). The gas to dust coupling has been neglected.

A. 1.1 *Extent of the ionized region*

The size of the HII region has been calculated by considering photoionization and recombination of hydrogen, along with the absorption due to the dust grains. The presence of the dust reduces the size of the ionized region, ($R_{\rm HII}$), compared to that of pure gas Stromgren sphere considerably, depending on the density and the gas to dust ratio. The dust grains can exist in principle, only beyond a radial distance, say $r_{\rm subl}$, depending on its sublimation temperature and the radiation field due to the central source. In practice, the actual distance beyond which the dust exists, say $r_{\rm fit,}$ is determined by the model fitting of the observed SED, by radiative transport calculations through the dust (D1(DL) or D1(MMP)). The $r_{\rm fit}$ is often much larger than $r_{\rm subl.}$

Hence, whether one encounters a dusty Stromgren sphere or not, is determined by the type of the star/integrated spectrum of the cluster; radial density distribution around the central star; and $r_{\rm fit.}$ We call it Case A, if the ionized region extends into the region where gas and dust coexist. The other case of entire ionized region devoid of any dust grains is termed Case B. So for Case B, the extent of the HII region can be obtained by solving the equation,

$$-\mathrm{d}N(r) = 4\pi\alpha_2 r^2 n_e^2(r)\mathrm{d}r \tag{1}$$

where, N is the number of Lyman continuum photons, α_2 is the recombination coefficient for hydrogen (for recombinations to all states except the ground state) and n_e is the number density of electrons or H^+ ions (for a pure HII region), which in our case is the gas number density (n_g) and may be given by,

$$n_g = n_0^{'}\left(\frac{R_{\rm min}}{r}\right)^m, \quad m = 0, 1, 2. \tag{2}$$

For m = 0,1,2 equation (1) can be solved easily by using the boundary condition

$$\text{at} \quad r = r_*, \quad N(0) = N_{\rm Lyc} \tag{3}$$

where, $N_{\rm Lyc}$ is the total number of Lyman continuum photons emitted per second by the embedded exciting star/star cluster and r_* is an effective stellar radius (with volume equal to the sum of that of all the stars of the embedded cluster; as it turns out, results are extremely insensitive to r_*).

In case A however, the ionizing (Lyman continuum) photons experience further attenuation due to direct absorption by the dust, so the modified radiation transfer equation would be,

$$-{\rm d}N(r) = 4\pi r^2 \alpha_2 n_e^2 {\rm d}r + N(r)\tau_{\rm Lyc}{\rm d}r \tag{4}$$

where $\tau_{\rm Lyc}$ refers to the optical depth of dust at $\lambda < 912$ Å. We solve the above equation, using the boundary conditions,

$$\text{at} \quad r = R_{\rm min}, \quad N(R_{\rm min}) = N_1 \tag{5}$$

where N_1 is determined by using equation (1) and

$$\text{at} \quad r = R_{\rm HII}, \quad N(R_{\rm HII}) = 0 \tag{6}$$

A. 1.2 *Calculation of continuum emission*

With $R_{\rm HII}$ properly determined, the radio continuum emission which occurs due to the free-free emission from the ions and electrons can be calculated by using the formula (Spitzer 1978),

$$J_\nu = \int_{r_*}^{R_{\rm HII}} 4\pi r^2 (4\pi\epsilon_\nu) e^{-\int_r^{R_{\rm HII}} \kappa_\nu {\rm d}r} {\rm d}r \tag{7}$$

where, the coefficients of emission ε_ν and absorption k_ν are respectively given by,

$$\epsilon_\nu({\rm erg/cm^3/sec/sr/Hz}) = 5.44 \times 10^{-39} g_{ff} Z_i^2 n_e n_i T^{-0.5} e^{-h\nu/kT} \tag{8}$$

$$\kappa_\nu(1/{\rm cm}) = 0.1731(1 + 0.130\log(T^{3/2}\nu^{-1}))Z_i^2 n_e n_i T^{-3/2}\nu^{-2} \tag{9}$$

with, Gaunt factor (*gff)* given by,

$$g_{ff} = 9.77(1 + 0.130\log(T^{3/2}\nu^{-1})). \tag{10}$$

An electron temperature of 8000 K has been assumed for all calculations. The radio continuum emission is computed at different frequencies depending on the availability of measurements for the particular astrophysical source under study. The frequencies are typically between 5 and 10 GHz.

References

Afflerbach, A., Churchwell, E., Werner, M. W. 1997, *Astrophys. J.,* **478**, 190 (ACW).

Aller, L. H., Liller, W. 1968, *Stars and Stellar Systems,* **Vol. VII**, 483.

Altenhoff, W. J., Downes, D., Pauls, T., Schraml, J. 1979, *Astr Astrophys. (Suppl)*, **35**, 23.

Baldwin, J., Ferland, G. J., Martin, P. G. *et al.* 1991, *Astrophys. J.,* **374**, 580.

Becker, R. H., White, R. L., Helfand, D. J., Zooneraatkermani, S. 1994, *Astrophys. J. Suppl*., **91**, 347.

Brand, J.,Cesaroni, R., Caselli, P. *et al.* 1994, *Astr. Astrophys.* (*Suppl*)*,* **103**, 541.

Bronfman, L.,Nyman,L.-A., May,J.1996, *Astr. Astrophys. (Suppl)*,**115**, 81.
Butner, H. M., Evans, N. J., Lester, D. F, Levreault, R. M., Strom, S. E. 1994, *Astrophys. J.,* **420**,326.
Chan, S. J., Henning, T., Schreyer, K. 1996, *Astr. Astrophys. (Suppl),* **115**, 285.
Chini, R., Kreysa, E., Mezger, P. G., Gemund, H. P. 1986, *Astr. Astrophys.,* **154**, L8.
Chini, R., Krugel, E., Wargau, W. 1987, *Astr. Astrophys.,* **181**, 378.
Churchwell, E.,Walmsley, C. M.,Cesaroni, R.1990, *Astr. Astrophys. (Suppl),***83**, 119.
Codella, C, Felli, M., Natale, V. 1996, *Astr. Astrophys.*, **311**, 971.
Codella, C, Palumbo, G. G. C., Pareschi, G., Scappini, R, Caselli, P., Attolini, M. R. 1995, *Mon. Not. R. Astr. Soc.,* **276**, 57.
Dartois,E., d'Hendecourt, L.,Boulanger, R *et al.* 1998, *Astr. Astrophys.*, **331**, 651.
de GraauwTh., Haser,L.N., Beintema,D. A. *et al.* 1996, *Astr. Astrophys.*, **315**, L49.
D'Hendecourt, L., Jourdain de Muizon, M., Dartois, E. *et al.* 1996, *Astr. Astrophys.*, **315**, L365.
Draine, B. T., Lee, H. M., 1984, *Astrophys. J.*, **285**, 89 (DL).
Egan, M. P., Leung, C. M., Spagna, G. R1988, *Computer Physics Communications*,**48**,271.
Faison, M., Churchwell, E., Hofner, P., Hackwell, J., Lynch, D. K., Sussell, R. W. 1998, *Astrophys. J.*, **500**, 280.
Ferland, G. J. 1996, *Hazy*, a brief introduction to CLOUDY, Univ. of Kentucky, Dept. of Phys. and Astron. Internal Reports.
Garay, G., Rodriguez, L. R, Moran, J. M., Churchwell, E. 1993, *Astrophys. J.*, **418**, 368.
Griffith, M. R., Wright, A. E., Burke, B. F, Ekers, R. D. 1995, *Astrophys. J. (Suppl),* **97**, 347.
Handa, T., Sofue, Y, Nakai, N., Hirabayashi, H., Inoue, M. 1987, *PASJ*, **39**, 709.
Haynes, R. R, Caswell, J. L., Simons, L. W. J. 1979, *Aust. J. Phys. Astrophys. (Suppl),* No. 48.
Jenness, T., Scott, P. F, Padman, R. 1995, *Mon. Not. R. Astr. Soc*, **276**, 1024.
Jourdain de Muizon, M., Cox, P., Lequeux, J. 1990, *Astr. Astrophys. (Suppl)*, **83**, 337.
Kurtz, S., Churchwell, E., Wood, D. O. S. 1994, *Astrophys. J. (Suppl)*, **91**, 659.
Laor, A., Draine, B. T. 1993, *Astrophys. J.*, **402**, 441.
Mathis, J.S.,Mezger, P. G.,Panagia, N. 1983, *Astr. Astrophys.*, **128**, 212.
Mathis, J. S., Rumpl, W., Nordsieck, K. H. 1977, *Astrophys. J.*, **217**, 425.
McCutcheon, W. H., Dewdney, P. E., Purton, R., Sato, T. 1991, *Astr. J.*, **101**, 1435.
McCutcheon, W. H., Sato, T., Purton, C. R., Matthews, H. E., Dewdney, P. E. 1995, *Astr. J.*, **110**, 1762.
Mezger, P. G., Mathis, J. S., Panagia, N. 1982, *Astr. Astrophys.*, **105**, 372 (MMP).
Molinari, S., Brand, J., Cesaroni, R., Palla, R 1996, *Astr. Astrophys.*, **308**, 573.
Osterbrock, D.E.,Tran, H. D.,Veilluex, S.1992, *Astrophys. J.*, **389**, 305.
Rubin, R. H., Simpson, J. R., Haas, M. R., Erickson, E. F. 1991, *Astrophys. J.*, **374**, 564.
Schutte, A. J., van der Walt, D. J., Gaylard, M. J., Macleod, G. C. 1993, *Mon. Not. R. Astr. Soc*, **261***,* 783.
Simpson, J. P., Rubin, R. H. 1990, *Astrophys. J*, **354**, 165 (SR).
Spitzer, L. 1978, *Physical Processes in the Interstellar Medium*, p.57.
Swinyard, B. M., Clegg, P. E., Ade, P. A. R. *et al.* 1996, *Astr. Astrophys.*, **315**, L43.
van der Walt, D.J., Gaylard, M. J., Macleod, G.C.1995, *Astr. Astrophys. (Suppl)*, **110**, 81.
Volk, K., Cohen, M. 1989, *Astr. J.,* **98**, 931.
Wood, D. O. S., Handa, T., Fukui, Y, Churchwell, E., Sofue, Y., Iwata, T. 1988, *Astrophys. J.*, **326**, 884.
Zoonematkermani, S., Helfand, D. J., Becker, R. H., White, R. L., Perley, R. A. 1990, *Astrophys. J. (Suppl)*, **74**, 181.